

Supplementary Table 1. Tephra thicknesses reported in the literature for the Millennium eruption deposits.

Label	Location	Latitude	Longitude	Thickness (cm)	Reference	Comendite phase (cm)	Trachyte phase (cm)
P01	S67-J17	42.000	130.283	9	Machida & Arai (2003)		
P02	St. 6913	41.333	130.417	10	Machida & Arai (1983)		
P03	St. 6920	40.283	132.217	5	Machida & Arai (1983)		
P04	KH69-2-25	40.867	132.65	4	Machida & Arai (1983)		
P05	S67-13	40.767	133.2	9	Machida & Arai (2003)		
P06	KH69-2-23	41.35	134.435	16	Machida & Arai (1983); Machida & Arai (2003)	10.88	5.12
P07	P128	40.017	136.398	10	Machida & Arai (2003)		
P08	P129	40.745	136.938	0.1	Machida & Arai (1983)		
P09	KH77-3-M5	41.005	137.018	8	Machida & Arai (1983)		
P10	KH79-3-C2	41.873	137.657	11	Machida & Arai (1983)		
P11	GH89-4-20-2	41.147	138.002	9	Machida & Arai (2003)		
P12	KH84-3-11	41.423	138.26	7.4	Machida & Arai (2003)		
P13	V28-271	40.75	138.45	2	Machida & Arai (1983)		
P14	GH89-2-19	40.952	138.667	11	Machida & Arai (2003)		
P15	P130	41.998	138.668	3	Machida & Arai (1983)	1.74	1.26
P16	GH89-4-35	40.898	139.015	6	Machida & Arai (2003)		
P17	KH84-3-9	41.833	139.163	3.2	Machida & Arai (2003)		
P18	P82	40.895	142.278	0.2	Machida & Arai (1983)		
P19	P83	40.678	142.783	0.2	Machida & Arai (1983)		
P20	t* (Sea of Japan)	42.633	141.567	2	Machida & Arai (1983)		
P21	Tomakomai Port	42.767	141.6	1	Machida & Arai (1983)	0.86	0.14
P22	near Toya	42.466	140.55	1	Machida & Arai (1983)		
P23	n* (Sea of Japan)	42.183	140.667	4	Machida & Arai (1983)		
P24	I* (Sea of Japan)	41.883	141.083	5	Machida & Arai (1983)		
P25	k* (Sea of Japan)	41.516	140	4	Machida & Arai (1983)	2.84	1.16
P26	u* (Sea of Japan)	40.3	141.333	5	Machida & Arai (1983)		
P27	o* (Sea of Japan)	40.483	140.483	4	Machida & Arai (1983)		
P28	Kurili	46.71	151.66	1.5	Razjigaeva et al. (2020)		
P29	Russkij Island	42.996	131.847	3	Razjigaeva et al. (2020)		
P30	Shkotovskoe Plateau	43.393	132.795	2	Razjigaeva et al. (2020)		
P31	Sergeevskoe Plateau	43.504	133.382	1.5	Razjigaeva et al. (2020)		

P32	Muta Area	43.522	134.144	1	Razjigaeva et al. (2020)		
P33	Suigetsu, Japan	35.583	135.883	0.1	McLean et al. (2016)	0.097	0.003
P34	Kiritappu, Hokkaido	43.078	145.101	1	Nanayama et al. (2003)	1.00	0.00
P35	RK12-0151 (Lake Kushu)	45.007	145.001	0.00144*	Chen et al. (2019)	0.00094	0.0005
P36	Sihailongwan, China	42.283	126.6	0.00256*	Sun et al. (2015)	0.00041	0.00215
P37	Ichi-no-Megata	39.955	139.739	0.2	Okuno et al. (2011)	0.097	0.103
P38	Utasai Bog, Hokkaido	42.633	140.307	4	Hughes et al. (2013)	2.16	1.84
P39	Shiriuchi	41.63	140.427	3	Nakanishi et al. (2020)		
P40	Hinohama	41.781	141.1	4	Nakanishi et al. (2020)		
P41	Todohokke	41.838	141.139	4	Nakanishi et al. (2020)		
P42	Hanaura	42.301	140.271	2	Nakanishi et al. (2020)		
P43	Yamazaki	42.319	140.274	2	Nakanishi et al. (2020)		
P44	Nakanosawa	42.484	140.353	1	Nakanishi et al. (2020)		
P45	Oshamanbe	42.537	140.399	1	Nakanishi et al. (2020)		
P46	Kyoritsu	42.555	140.42	1	Nakanishi et al. (2020)		
P47	Arutori	42.503	140.798	2	Nakanishi et al. (2020)		
P48	Kogane	42.395	140.911	1	Nakanishi et al. (2020)		
P49	Wakayama	42.386	141.076	1	Nakanishi et al. (2020)		
P50	Tomiura	42.44	141.151	1	Nakanishi et al. (2020)		
P51	Shadai	42.56	141.376	1	Nakanishi et al. (2020)		
P52	Atsuma	42.617	141.782	1	Nakanishi et al. (2020)		
P53	Taura	42.581	141.905	3	Nakanishi et al. (2020)		
P54	Shiomi	42.555	141.939	1	Nakanishi et al. (2020)		
P55	Monbetsu	42.484	142.046	3	Nakanishi et al. (2020)		
P56	Toyosato	42.473	142.118	2	Nakanishi et al. (2020)		
P57	Kabari	42.448	142.196	2	Nakanishi et al. (2020)		
P58	Urawa	42.309	142.432	3	Nakanishi et al. (2020)		
P59	Higashisizunai	42.304	142.454	2	Nakanishi et al. (2020)		
P60	Harutachi	42.266	142.513	2	Nakanishi et al. (2020)		
P61	Kerimai W	42.228	142.614	2	Nakanishi et al. (2020)		
P62	Kerimai E	42.217	142.642	1	Nakanishi et al. (2020)		
P63	Efue	42.192	142.723	3	Nakanishi et al. (2020)		
P64	Utoma	42.137	142.86	4	Nakanishi et al. (2020)		
P65	Nishisamani	42.137	142.91	1	Nakanishi et al. (2020)		
P66	Tomabetsu	41.99	143.245	4	Nakanishi et al. (2020)		

P67	Syoya	41.998	143.253	5	Nakanishi et al. (2020)		
P68	Gushantun Peat	42.306	126.283	0.01	Zhao and Liu, 2012; Zhao et al., 2015	0.01	0.00
P69	Sea of Japan	40.53	132.2	5	Furuta et al. (1986); Machida and Arai, 1983	3.30	1.70
P70	Asahidake Volcano	43.65	142.85	1	Wada et al. (2001)	0.73	0.27
P71	Sapporo archaeological Site	43.067	141.35	0.1	Nakamura (2016)	0.08	0.02
P72	Tyatya Volcano, Kuril Arc	44.351	146.256	1	Nakagawa et al. (2002)	1.00	0.00
P73	Lake Ogawara	40.783	141.317	2	Fukusawa et al. (1988)	0.77	1.23
P74	13PT_P4 Ulleung Basin core	37.0144	130.266	0.038*	Chen et al. (2022)	0.038	0
P75	Komaga-take volcano	42.082	140.688	5	Wei et al. (2013)		
P76	Tumen River	42.014	128.42	100	Pan et al. (2020)		
P77	Tianwenfeng peak	42.02	128.069	150	Chen et al. (2016); Sun et al. (2017)	35	115
P78	Heishi River	42.05	128.242	60	Pan et al. (2020)	10	50
P79	Yuanchi	41.998	128.539	72	Pan et al. (2020) ^s	26	46
P80	Site 1, Fig. 12	42.011	128.423	90	Pan et al. (2020)	50	40
P81	Site 2, Fig. 12	42.033	128.421	50	Pan et al. (2020)	10	40
P82	Site 4, Fig. 12	42.074	128.416	50	Pan et al. (2020)	0.00	50
P83	Site 5, Fig. 12	42.113	128.376	20	Pan et al. (2020)	Not exposed	20
Vent		42.006	128.055	-	-		

Footnote: *These tephra layers are not visible and reported as shard concentrations. Thicknesses have been estimated for these layers assuming 25,000 shards/gram = 1 mm thickness, which is based on thickness and shard concentration in Lake Suigetsu (McLean et al., 2016). ^sChen et al. (2016) and Sun et al. (2017) glass chemistry show that Pan et al. (2020) assignment of the units (comendite vs trachyte) is not correct for the Tianwenfeng peak location, and that colour of the deposit can be used as a good measure of the composition. We can clearly see a light grey unit, followed by a slightly darker deposit at Yuanchi and have reduced Pan et al. (2020) thickness of the comendite from 45 cm to 26 cm (based on relative thickness on the photo in the paper) and extended the thickness of the trachytic deposit by 19 cm.

Tephra thicknesses from terrestrial exposures and marine and lake cores were used to model the tephra dispersal from the two phases of the Millennium Eruption. The reliability of core tephra data has been the focus of studies by Engwell et al., (2014) and Freundt et al. (2021). These studies identified that the accuracy of the thickness and bulk granulometry of these core deposits depends on various parameters relating to the coring and the setting but indicate that these core records are commonly more reliable than those on-land (Engwell et al., 2014, Freundt et al., 2021).

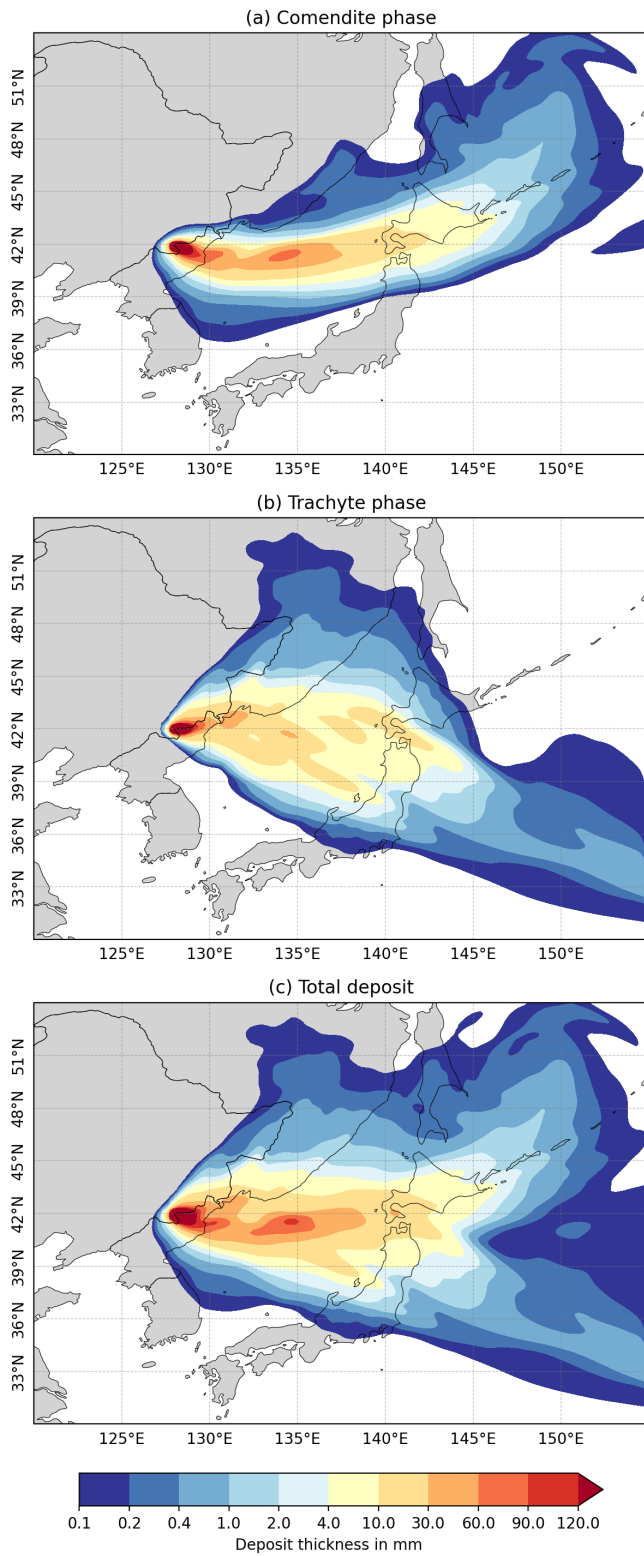
Supplementary References

1. Chen, X.-Y., Blockley, S.P., Tarasov, P.E., Xu, Y.G., McLean, D., Tomlinson, E.L., Albert, P.G., Liu, J.Q., Müller, S., Wagner, M. and Menzies, M.A. (2016) Clarifying the distal to proximal tephrochronology of the Millennium (B-Tm) eruption, Changbaishan Volcano, northeast China. *Quat Geochronol* **33**, 61-75.
2. Chen, X.-Y., Blockley, S. P. E., Fletcher, R., Zhang, S., Kim, J.-H., Park, M.-H., Chen, C., Yin, J., Yu Y.-G. (2022). Holocene tephrostratigraphy in the East Sea/Japan Sea: Implications for eruptive history of Ulleungdo volcano and potential for hemispheric synchronization of sedimentary archives. *J. Geophys. Res. Solid Earth* **127**: e2021JB023243
3. Fukusawa, H., Tsukamoto, S., Tsukamoto, H., Ikeda, M., Okamura, M. & Matsuoka, M. (1998) Falling age of Baegdusan-Tomakomai tephra (B-Tm) estimated by using non-glacial varves. *Laguna* **5**, 55-62.
4. Furuta, T., Fujioka, K. & Arai, F. (1986) Widespread submarine tephras around Japan- Petrographic and chemical properties. *Mar. Geol.* **72**, 125-142.
5. Hughes, P.D.M., Mallon, G., Brown, A., Essex, H.J., Stanford, J.D. & Hotes, S. (2013) The impact of high tephra loading on late-Holocene carbon accumulation and vegetation succession in peatland communities. *Quat. Sci. Rev.* **67**, 160-175.
6. Machida H, Arai F (1983) Extensive ash falls in and around the Sea of Japan from large late Quaternary eruptions. *J Volcanol Geotherm Res* **18** (1-4):151–164
7. Machida, H. and Arai, F., 2003, Atlas of tephra in and around Japan [Revised Edition]. University of Tokyo Press, Tokyo, 336p.
8. McLean, D., Albert, P.G., Nakagawa, T., Staff, R., Suzuki, T., Suigetsu 2006 Project Members and Smith, V.C., (2016) Identification of the Changbaishan 'Millennium' (B-Tm) eruption deposit in the Lake Suigetsu (SG06) sedimentary archive, Japan: synchronisation of hemispheric-wide palaeoclimate archives. *Quat Sci Rev* **150**: 301–307, doi:10.1016/j.quascirev.2016.08.022
9. Nakagawa, M., Ishizuka, Y., Kudo, T., Yoshimoto, M., Hirose, W., Ishizaki, Y., Gouchi, N., Katsui, Y., Solovyow, A.W., Steinberg, G.S. & Abdurakhmanov, A.I. (2002) Tyatya volcano, southwestern Kuril arc: recent eruptive activity inferred from widespread tephra. *Isl. Arc* **11**, 236-254.
10. Nakamura, Y. (2016) Stratigraphy, distribution, and petrographic properties of Holocene tephras in Hokkaido, northern Japan. *Quat. Int.* **397**, 52-62.
11. Nakanishi, R., Okamura, S., Yokoyama, Y., Miyairi, Y., Sagayama, T. & Ashi, J. (2020) Holocene tsunami, storm, and relative sea level records obtained from the southern Hidaka coast, Hokkaido, Japan. *Quat. Sci. Rev.* **250**, 106678.
12. Nanayama, F., Satake, K., Furukawa, R., Shimokawa, K., Atwater, B.F., Shigeno, K. and Yamaki, S., (2003), Unusually large earthquakes inferred from tsunami deposits along the Kuril trench. *Nature* **424**: 660-663.
13. Okuno, M., Torii, M., Yamada, K., Shinohara, Y., Danhara, T., Gotanda, K., Yonenobu, H. & Yasuda, Y. (2011) Widespread tephras in sediments from Lake Ichi-no-Megata in northern Japan: their description, correlation and significance. *Quat. Int.* **246**: 270-277.
14. Pan, B., de Silva, S.L., Xu, J., Liu, S. and Xu, D., (2020) Late Pleistocene to present day eruptive history of the Changbaishan-Tianchi Volcano china/DPRK: New field, geochronological and chemical constraints. *J Volcanol Geotherm Res* **399**: 106870
15. Razjigaeva, N.G., Ganzei, L.A., Makarova, T.R., Korniyushenko, T.V., Ganzei, K.S., Sudin, V.V. & Kharlamov, A.A. (2020) Paleolake of Shkot Island (Peter the Great Gulf): Natural archives of climatic and landscape vegetation, *Geosyst. Transition Zones* **4**, 230–249. (In Russ.)
16. Sun, C., You, H., He, H., Zhang, L., Gao, J., Guo, W., Chen, S., Mao, Q., Liu, Q., Chu, G. & Liu, J. (2015) New evidence for the presence of Changbaishan Millennium eruption ash in the Longgang volcanic field, Northeast China. *Gondwana Res.* **28**, 52-60.
17. Sun, C., Liu, J., You, H., Németh, K., (2017) Tephrostratigraphy of Changbaishan volcano, northeast China, since the mid-Holocene. *Quat. Sci. Rev.* **177**, 104–119.
18. Wada, K., Nakamura, M. & Okuno, M. (2001) Identification of source volcano from the chemical Compositions of glasses from the widespread ashes in the surface layers of Asahidake volcano, Central Hokkaido, Japan. *Rep. Taisetsuzan Inst. Sci.* **35**, 9-18 . (In Japanese)
19. Wei, H., Liu, G. & Gill, J. (2013) Review of eruptive activity at Tianchi volcano, Changbaishan, northeast China: implications for possible future eruptions. *Bull Volcanol*, **75**, 760, 1-14.
20. Zhao, H.L., Liu, J.Q. (2012) Cryptotephra discovered in Gushantun peat of the China and its significance. *Seismol and Geol* **34**: 516–530 (in Chinese).
21. Zhao, H.L., Li, X.Q., Hall, V.A. (2015) Holocene vegetation change in relation to fire and volcanic events in Jilin, Northeastern China. *Sci. China Earth Sci.* **58**, 1404–1419.

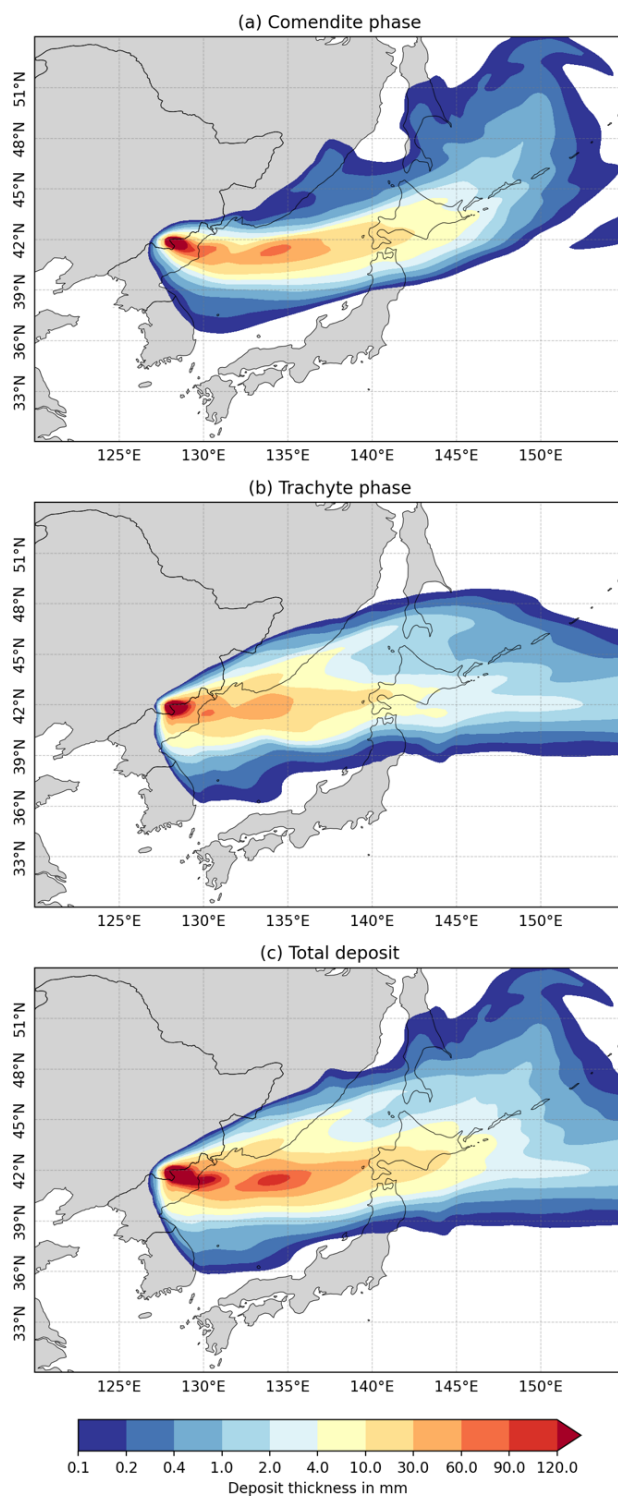
22. Engwell, S.L., Sparks, R.S.J., Carey, S. (2014) *Physical characteristics of tephra layers in the deep sea realm: the Campanian Ignimbrite eruption*. In: Marine Tephrochronology. Austin W.E.N., Abbott P.M., Davies S.M., Pearce N.J.G., Wastegard S (eds), vol. Geological Society, London, Special Publications, p 398, 47–64.
23. Freundt, A., Schindlbeck-Belo, J.C., Kutterolf, S., Hopkins, J. L. (2023) *Tephra layers in the marine environment: a review of properties and emplacement processes*. In: Volcanic Processes in the Sedimentary Record: When Volcanoes Meet the Environment. Di Capua, A., De Rosa, R., Kereszturi, G., Le Pera, E., Rosi, M. Watt, S. F. L. (eds). Geological Society, London, Special Publications, 520.

Supplementary Table 2:

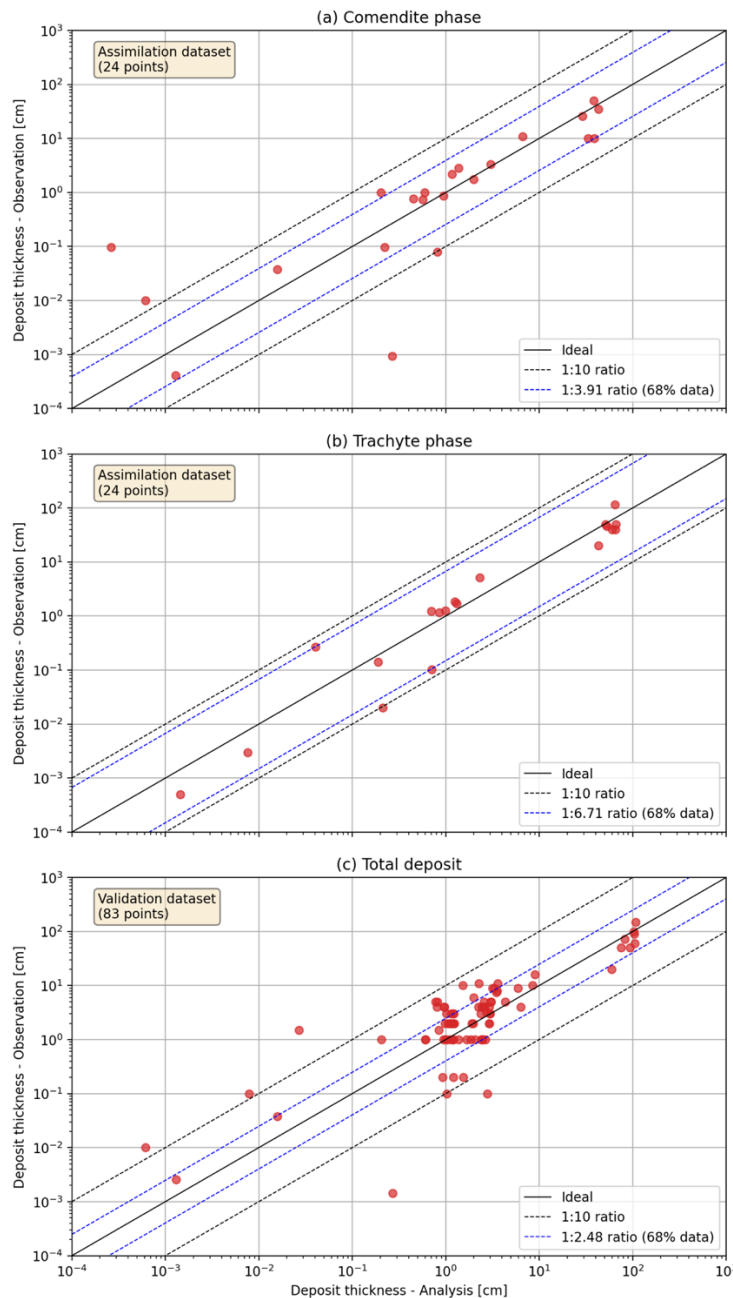
Meteorological configuration for the comendite phase	Meteorological configuration for the trachyte phase	RMSE	BIAS	MAE	SMAPE	CR (68.67% band)	CI (RMSE+BIAS+MAE+CR+SMAPE/100)
19680930-19681004	19680930-19681004	1.228	0.779	0.944	47.528	4.130	7.556
19680930-19681004	19751008-19751012	1.321	0.815	0.995	48.485	4.880	8.496
19680930-19681004	19781129-19781203	1.154	0.643	0.841	39.412	3.710	6.742
19680930-19681004	19860923-19860927	1.166	0.666	0.859	39.631	3.370	6.457
19680930-19681004	19921030-19921103	1.156	0.655	0.845	39.195	3.130	6.178
19680930-19681004	19940421-19940425	1.139	0.645	0.863	44.376	4.720	7.811
19751008-19751012	19680930-19681004	1.270	0.825	0.949	45.813	4.520	8.022
19751008-19751012	19751008-19751012	1.411	0.861	1.055	51.754	7.540	11.384
19751008-19751012	19781129-19781203	1.246	0.689	0.914	42.921	3.820	7.098
19751008-19751012	19860923-19860927	1.219	0.712	0.889	39.650	3.410	6.625
19751008-19751012	19921030-19921103	1.227	0.701	0.902	41.908	3.330	6.579
19751008-19751012	19940421-19940425	1.218	0.691	0.940	48.792	5.000	8.336
19781129-19781203	19680930-19681004	1.101	0.551	0.822	37.873	3.110	5.963
19781129-19781203	19751008-19751012	1.242	0.588	0.918	41.879	3.430	6.597
19781129-19781203	19781129-19781203	1.158	0.415	0.870	38.961	3.040	5.873
19781129-19781203	19860923-19860927	1.117	0.438	0.850	37.793	2.680	5.463
19781129-19781203	19921030-19921103	1.127	0.427	0.852	38.056	2.640	5.427
19781129-19781203	19940421-19940425	1.102	0.417	0.854	40.227	3.060	5.835
19860923-19860927	19680930-19681004	1.037	0.526	0.772	34.650	2.470	5.151
19860923-19860927	19751008-19751012	1.157	0.563	0.853	36.966	2.570	5.513
19860923-19860927	19781129-19781203	1.052	0.390	0.785	33.924	2.380	4.946
19860923-19860927	19860923-19860927	1.056	0.413	0.781	35.580	2.390	4.996
19860923-19860927	19921030-19921103	1.053	0.402	0.779	34.580	2.170	4.751
19860923-19860927	19940421-19940425	1.005	0.392	0.766	35.273	2.480	4.996
19921030-19921103	19680930-19681004	1.045	0.541	0.780	35.721	2.630	5.353
19921030-19921103	19751008-19751012	1.171	0.578	0.872	39.718	2.920	5.938
19921030-19921103	19781129-19781203	1.054	0.405	0.799	35.930	2.500	5.118
19921030-19921103	19860923-19860927	1.048	0.428	0.787	35.469	2.200	4.818
19921030-19921103	19921030-19921103	1.053	0.417	0.793	36.828	2.350	4.981
19921030-19921103	19940421-19940425	1.020	0.407	0.790	38.272	2.740	5.339
19940421-19940425	19680930-19681004	1.137	0.646	0.863	44.366	4.660	7.749
19940421-19940425	19751008-19751012	1.281	0.683	0.991	51.841	5.610	9.083
19940421-19940425	19781129-19781203	1.154	0.510	0.889	43.394	3.560	6.546
19940421-19940425	19860923-19860927	1.071	0.533	0.831	39.327	2.950	5.778
19940421-19940425	19921030-19921103	1.092	0.522	0.848	42.091	3.160	6.042
19940421-19940425	19940421-19940425	1.219	0.512	0.966	50.767	5.810	9.014



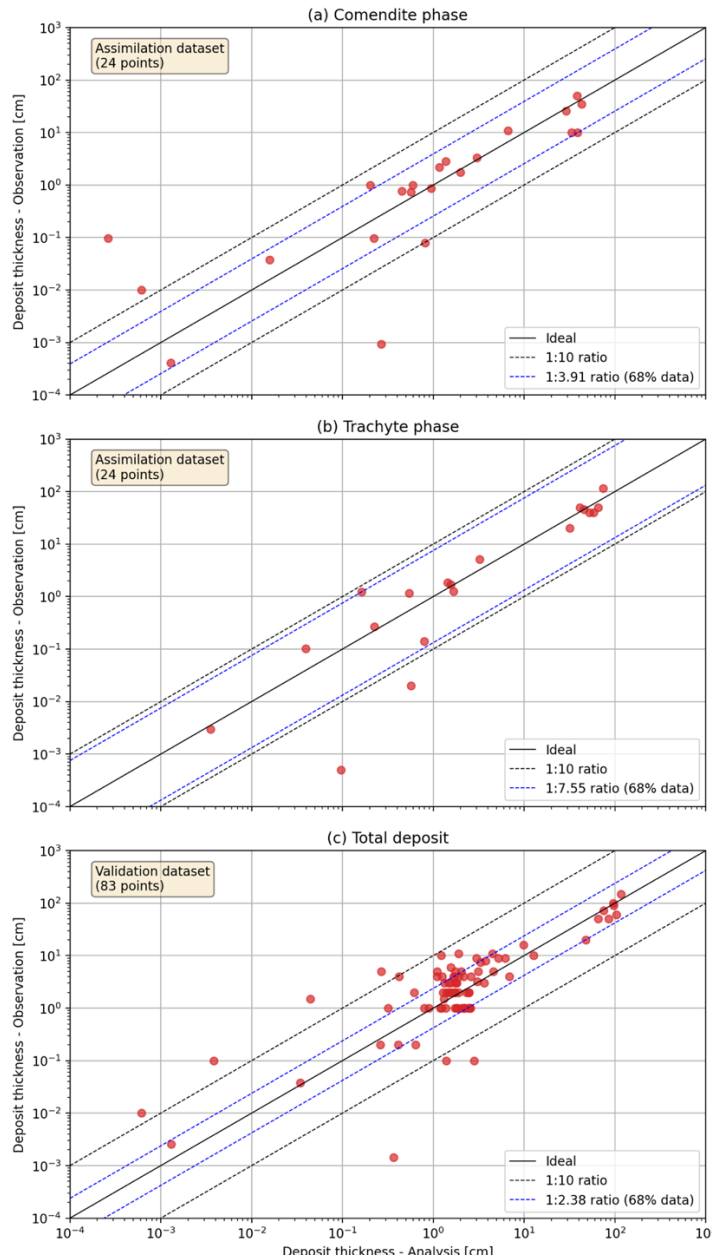
Supplementary Figure 1. Reconstructed deposit thickness contours for the comendite (a), trachyte (b) eruptive phases, and for the total deposit (c) of the Millennium Eruption (ME), for the simulations using the meteorological condition of 23 September 1986 for the comendite phase and 21 April 1994 for the trachyte phase. The maps were created using the open software “Cartopy: a cartographic python library with a matplotlib interface” (<https://scitools.org.uk/cartopy/docs/latest/index.html>).



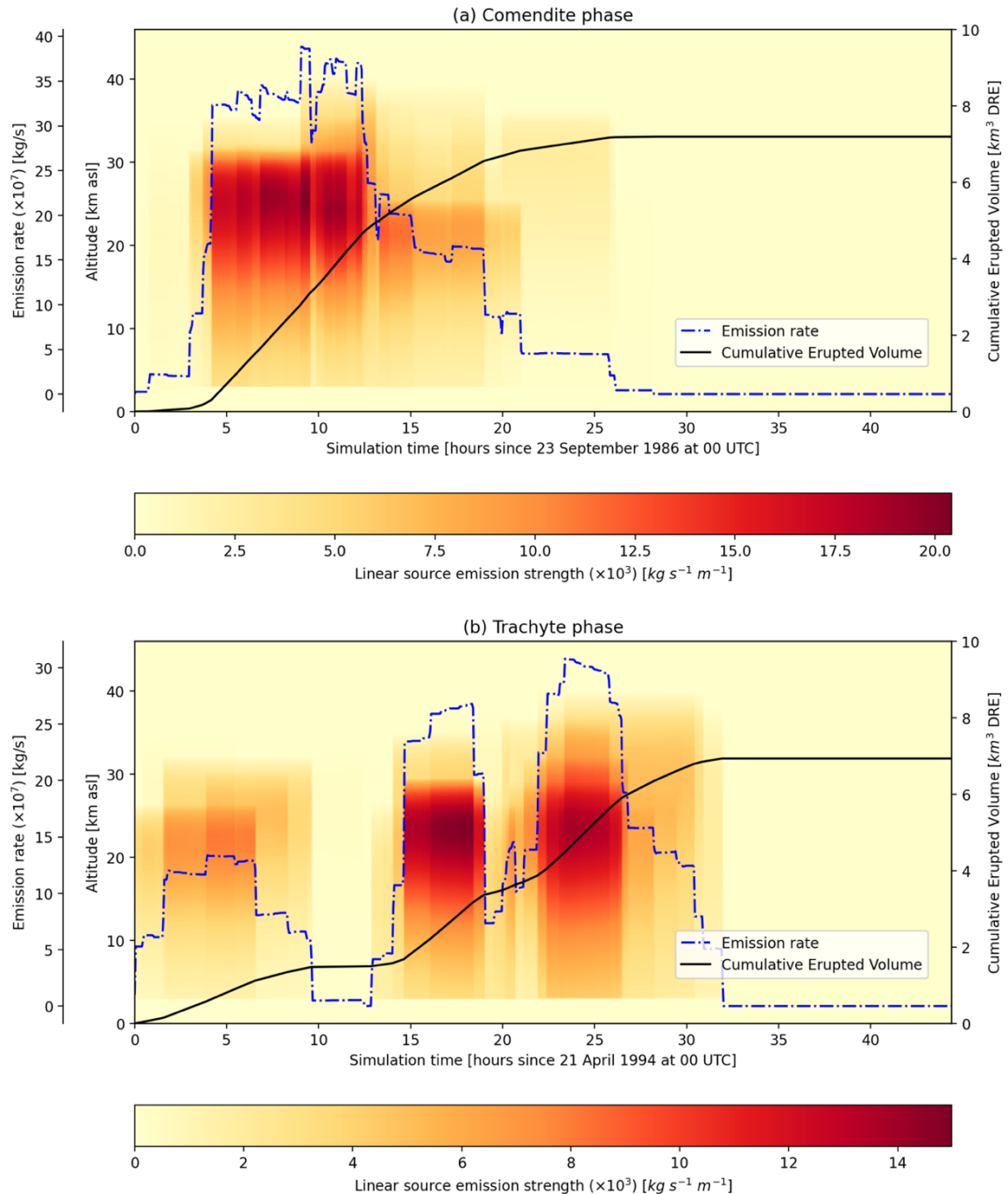
Supplementary Figure 2. Reconstructed deposit thickness contours for the comendite (a), trachyte (b) eruptive phases, and for the total deposit (c) of the Millennium Eruption (ME), for the simulations using the meteorological condition of 23 September 1986 for the comendite phase and 29 November 1978 for the trachyte phase. The maps were created using the open software “Cartopy: a cartographic python library with a matplotlib interface” (<https://scitools.org.uk/cartopy/docs/latest/index.html>).



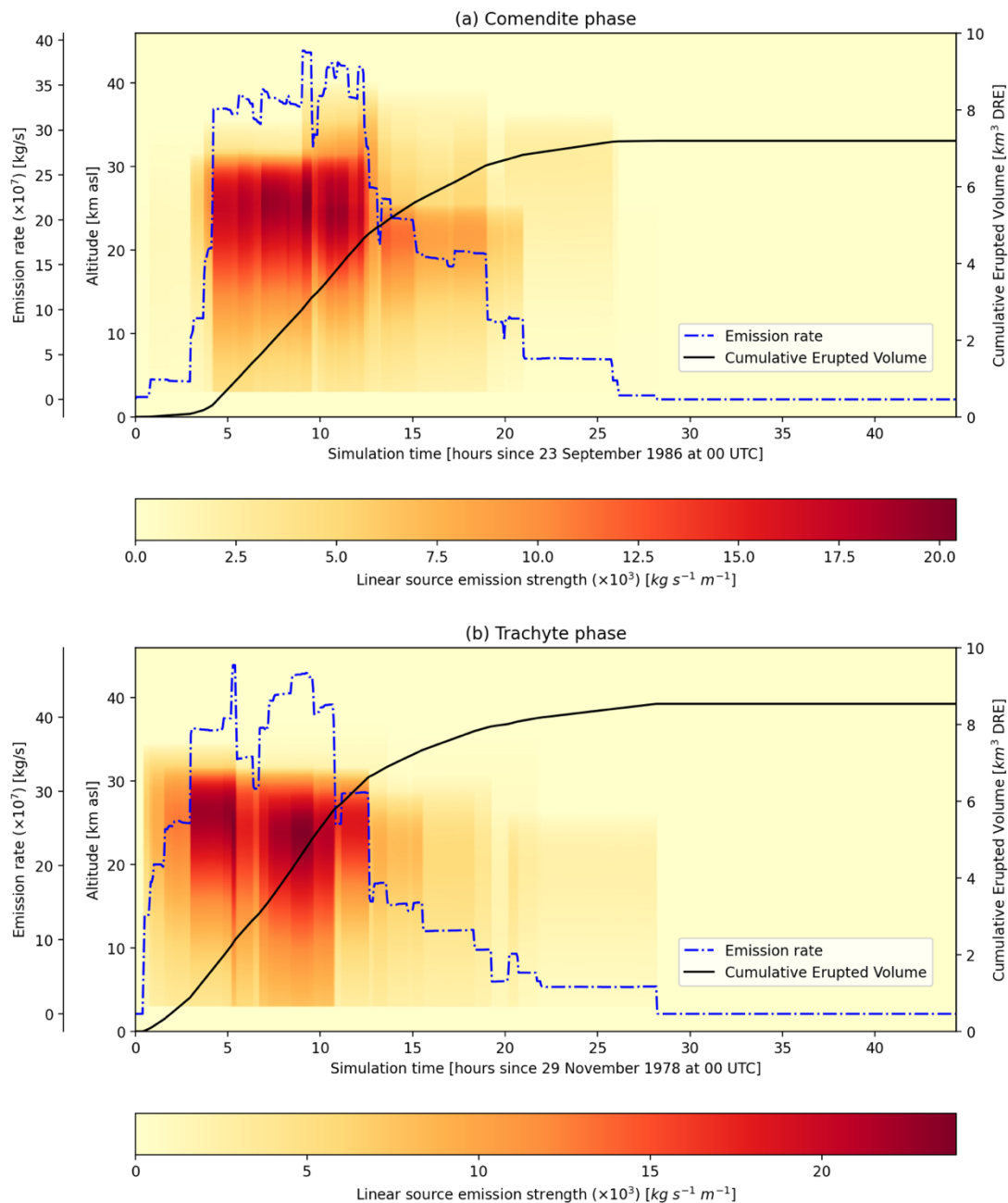
Supplementary Figure 3. Quantitative comparison between observed and modelled (analysis) deposit thickness of the comendite (a) and trachyte (b) eruptive phases of the Millennium Eruption (ME) using the assimilation dataset (23 measurements for each eruptive phase). In addition, the comparison between the total deposit thickness and the validation dataset (83 measurements) is also shown (c), for the simulations using the meteorological condition of 23 September 1986 for the comendite phase and 21 April 1994 for the trachyte phase. The plots were created using the open software Matplotlib (<https://matplotlib.org/stable/>).



Supplementary Figure 4. Quantitative comparison between observed and modelled (analysis) deposit thickness of the comendite (a) and trachyte (b) eruptive phases of the Millennium Eruption (ME) using the assimilation dataset (23 measurements for each eruptive phase). In addition, the comparison between the total deposit thickness and the validation dataset (83 measurements) is also shown (c), for the simulations using the meteorological condition of 23 September 1986 for the comendite phase and 23 September 1986 for the comendite phase and 29 November 1978 for the trachyte phase. The plots were created using the open software Matplotlib (<https://matplotlib.org/stable/>).



Supplementary Figure 5. Time evolution of the emission source profiles derived for the comenditic first phase (a) and trachytic phase (b) of the Millennium Eruption (ME), for the simulations using the meteorological condition of 23 September 1986 for the comendite phase and 21 April 1994 for the trachyte phase. The plots were created using the open software Matplotlib (<https://matplotlib.org/stable/>).



Supplementary Figure 6. Time evolution of the emission source profiles derived for the comenditic first phase (a) and trachytic phase (b) of the Millennium Eruption (ME), for the simulations using the meteorological condition of 23 September 1986 for the comendite phase and 29 November 1978 for the trachyte phase. The plots were created using the open software Matplotlib (<https://matplotlib.org/stable/>).